Functionalized Rhodium Intercalators for DNA Recognition

Robert H. Terbrueggen,† Timothy W. Johann,‡ and Jacqueline K. Barton*

Division of Chemistry and Chemical Engineering, California Institute of Technology, Pasadena, California 91125

Received July 17, 1998

A series of rhodium complexes containing the phenanthrenequinone diimine (phi) ligand have been prepared which bind DNA by intercalation and, upon photoactivation, promote DNA strand breaks. In this series, the ancillary, nonintercalating bipyridyl or phenanthroline ligands have been functionalized to yield complexes containing guanidinium, amido, or amino groups arranged with defined stereochemistry for site-specific interaction with the DNA bases. Λ-1-$[Rh(MGP)_2phi]^{5+}$ (MGP = 4-(guanidylmethyl)-1,10-phenanthroline) site-specifically targets the 6-base pair sequence 5′-CATATG-3′ with a binding affinity of 1 (±0.5) × 10^8 M^{-1} while Δ-1-$[Rh(MGP)_2phi]^{5+}$ displays an affinity of 5 (±2) × 10^7 M^{-1} for 5′-CATCTG-3′. Even though these two isomers target sites which differ by only a single base, binding is highly enantioselective. The specificity is derived chiefly from interactions of the pendant guanidinium groups with the DNA bases. For the racemates of 1-$[Rh(GEB)_2phi]^{5+}$ (GEB = (4-(2-guanidylethyl)-4′-methyl-2,2′-bipyridine) and 1-$[Rh(GPB)_2phi]^{5+}$ (GPB = (4-(2-guanidylpropyl)-4′-methyl-2,2′-bipyridine), photocleavage patterns also show the strongest site of photocleavage as 5′-CATCTG-3′, the target site for Δ-1-$[Rh(MGP)_2phi]^{5+}$. Moreover, consistent with the dominance of the guanidinium groups in establishing specificity, significantly enhanced photocleavage is evident for the 1-positional isomer of these complexes, where the guanidinium moieties are directed toward the DNA (above and below the phi ligand) compared to the 2-isomer, in which the guanidinium groups are directed away from the DNA. In contrast to Λ-1-$[Rh(MGP)_2phi]^{5+}$, Λ-1-$[Rh(GEB)_2phi]^{5+}$ shows little cleavage at 5′-CATATG-3′; this sensitivity to linker length likely depends on the mode of recognition of 5′-CATATG-3′ involving sequence-dependent unwinding of the DNA site. Analogous site-specificity or isomer-specificity is not evident with the complexes which contain pendant amido or amino functionalities. Instead these complexes appear to resemble the parent, unfunctionalized $[Rh(phen)_2phi]^{3+}$ with respect to recognition. Pendant guanidinium functionalities appear to be particularly advantageous in the construction of small molecules which bind DNA with site-specificity.

Introduction

The ability to design molecules rationally which are capable of targeting specific DNA sites offers attractive possibilities in developing both pharmaceuticals and tools for biotechnology.[1,2] Our laboratory has focused on exploring the DNA recognition characteristics of a unique class of DNA-binding agents, phenanthrenequinone diimine (phi) complexes of rhodium(III).[3−10] Phi complexes of rhodium(III) bind to B-DNA via intercalation of the phi ligand into the major groove and promote strand scission upon photoactivation. The intercalative stacking of the phi ligand yields large DNA binding affinities (>10^6 M^{-1}) for this family of complexes. Phi ligand intercalation into double-stranded DNA appears to be a relatively nonspecific interaction, and it is instead the ensemble of noncovalent contacts by the nonintercalating ancillary ligands of the octahedral metal complex which determine its sequence-specificity. Thus intercalation by these metallointercalators provides a basis for orienting a range of contacts in the DNA major groove and hence an opportunity to explore the principles of recognition of the DNA helix systematically.

We have previously reported the construction of phi complexes of rhodium(III) whose DNA recognition characteristics are governed either by direct readout, indirect readout (shape selection), or a combination of these. For example, in mimicking the direct readout of DNA sequences by proteins, Δ-Δ-$[Rh[(R,R)\text{-}Me_2trien]phi]^{3+}$ (Me_2trien = 2,9-diamino-4,7-diazadecane), has been shown to recognize the predicted sequence 5′-TGCA-3′ through a mixture of hydrogen bonds and van der Waals contacts.[7] $[Rh(phen)_2phi]^{3+}$, in contrast, recognizes open major groove sites through shape-selection,[4,9] and indeed shape-

* To whom correspondence should be addressed.
† Present address: Clinical Micro Sensors, Pasadena, CA.
‡ Present address: Incyte Pharmaceuticals, Palo Alto, CA.

(1) (a) Johann, T. W.; Barton, J. K. *Philos. Trans. R. Soc. London A* **1996**, *354*, 299 and references therein.
(2) Chow, C. S.; Barton, J. K. *Methods Enzymol*. **1992**, *212*, 219.
(3) (a) Pyle, A. M.; Long, E. C.; Barton, J. K. *J. Am. Chem. Soc.* **1989**, *111*, 4520−4522. (b) Krotz, A. H.; Kuo, L. Y.; Barton, J. K. *Inorg. Chem.* **1993**, *32*, 5963.
(4) Sitlani, A.; Long, E. C.; Pyle, A. M. Barton, J. K. *J. Am. Chem. Soc.* **1992**, *114*, 2303.
(5) (a) Krotz, A. H.; Kuo, L. Y.; Shields, T. P.; Barton, J. K. *J. Am. Chem. Soc.* **1993**, *115*, 3877. (b) Sitlani, A.; Barton, J. K. *Biochemistry* **1994**, *33*, 12100. (c) Collins, J. G.; Shields, T. P.; Barton, J. K. *J. Am. Chem. Soc.* **1994**, *116*, 9840. (d) Shields, T. P.; Barton, J. K. *Biochemistry* **1995**, *34*, 15049. (e) Shields, T. P.; Barton, J. K. *Biochemistry* **1995**, *34*, 15037.
(6) David, S. S.; Barton, J. K. *J. Am. Chem. Soc.* **1993**, *115*, 2984.
(7) (a) Krotz, A. H.; Hudson, B. P.; Barton, J. K. *J. Am. Chem. Soc.* **1993**, *115*, 12577. (b) Hudson, B. P.; Dupureur, C. M.; Barton, J. K. *J. Am. Chem. Soc.* **1995**, *117*, 9379. (c) Hudson, B. P.; Barton, J. K. *J. Am. Chem. Soc.* **1998**, *120*, 6877.
(8) Sardesai, N. Y.; Zimmerman, K.; Barton, J. K. *J. Am. Chem. Soc.* **1994**, *116*, 7502.
(9) Campisi, D.; Morii, T.; Barton, J. K. *Biochemistry* **1994**, *33*, 4130.
(10) Sitlani, A.; Dupureur, C. M.; Barton, J. K. *J. Am. Chem. Soc.* **1993**, *115*, 12589.

10.1021/ic980837j CCC: $15.00
Published on Web 12/03/1998

selection has been powerfully applied in targeting the 8-base pair sequence 5′-CTCTAGAG-3′ by Δ-[Rh(diphenylbpy)$_2$phi]$^{3+}$.[10]

Here we describe our efforts to explore more fully the combination of direct and indirect readout of DNA through the construction of derivatives of [Rh(phen)$_2$phi]$^{3+}$ and [Rh(bpy)$_2$phi]$^{3+}$ which contain appended functionality on the phenanthroline or bipyridine ligands with defined stereochemistry. In an array of DNA binding proteins, the guanidinium side chain of arginine residues is commonly used to target guanines.[11,12] In addition, DNA mutagenesis experiments, crystal structures, and NMR solution structures of protein/DNA complexes have demonstrated that the amino group and the amido group contribute to sequence-determining contacts.[11,13] The amido moiety may specifically contact adenines by forming a bidentate hydrogen bond with N7 and C6 amino group of adenine. The amino group from the side chain of lysine can act as a general proton donor for hydrogen bonding interactions, yet this side chain has been seen primarily in specific hydrogen bonding contacts with guanine. Here we examine the DNA photocleavage properties of phi complexes of rhodium(III) which possess tethered amine and amide functionalities, as well as guanidylethyl and guanidylpropyl moieties.

A striking example of recognition through a combination of direct and indirect readout of DNA is evident in the construction of the metallointercalator, Λ-1-[Rh(MGP)$_2$phi]$^{5+}$ [MGP = 4-(guanidylmethyl)-1,10-phenanthroline], shown in Figure 1.[14] Λ-1-[Rh(MGP)$_2$phi]$^{5+}$ specifically targets the site 5′-CATATG-3′ at nanomolar concentrations. An essential feature of this recognition is the sequence-specific unwinding of the DNA helix, which permits direct contacts between guanidinium functionalities on the complex and guanine residues. Complex binding has been shown to require approximately a 70° unwinding of the DNA helix.[14]

The metal complex [Rh(amidoEB)$_2$phi]$^{3+}$ (amidoEB = 4-(2-amidoethyl)-4′-methylbipyridine) (Figure 1) represents an analogue of [Rh(MGP)$_2$phi]$^{5+}$ which potentially could employ the amido moiety instead of the guanidinium moiety for sequence-specific DNA contacts. The distance from the bipyridyl ring system to the terminal nitrogen of amide moiety is roughly equal to the distance from the phenanthroline ring to the terminal nitrogen of the guanidinium moiety in [Rh(MGP)$_2$phi]$^{5+}$. It is noteworthy, however, that the amido moiety is uncharged in neutral solution. The metal complex [Rh(aminoPB)$_2$phi]$^{5+}$ (aminoPB = 4-(3-aminopropyl)-4′-methylbipyridine), also shown in Figure 1, was prepared to determine if the DNA recognition seen for [Rh(MGP)$_2$phi]$^{5+}$ is unique to the guanidinium moiety or might be duplicated with a charged amino group. Importantly, the aminopropyl moiety is much more rotationally unrestrained than the guanidylmethyl moiety, and thus [Rh(aminoPB)$_2$phi]$^{5+}$ may also be used to explore how linker arm flexibility affects complex specificity. To directly compare linkers, we examine two additional metal complexes containing guanidinium functionalities, [Rh(GEB)$_2$phi]$^{5+}$ (GEB = (4-(2-guanidylethyl)-4′-methyl-2,2′-bipyridine) and [Rh(GPB)$_2$phi]$^{5+}$ (GPB = 4-(2-guanidylpropyl)-4′-methyl-2,2′-bipyridine). The stereochemical placement of these ancillary functionalities is well-defined in separated isomers of each complex. Therefore, the systematic comparison of the recognition properties of these complexes allows us to probe the importance of charge considerations, the importance of spatial positioning and flexibility of the functional group with respect to the metal, and indeed to begin to examine how hydrogen-bonding functional groups may be applied for predictable sequence-determining contacts in metallointercalators.

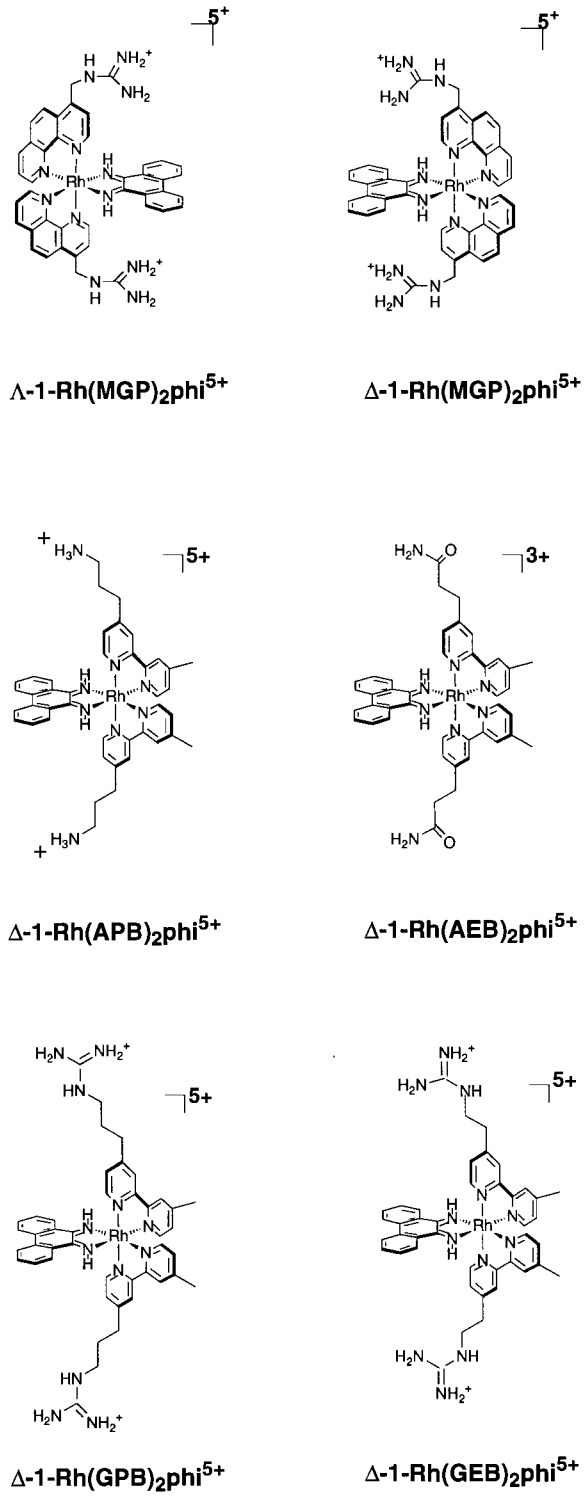

Figure 1. Schematic illustration of (top left) Λ-1-[Rh(MGP)$_2$phi]$^{5+}$, (top right) Δ-1-[Rh(MGP)$_2$phi]$^{5+}$, (center left) Δ-1-[Rh(aminoPB)$_2$phi]$^{5+}$, (center right) Δ-1-[Rh(amidoEB)$_2$phi]$^{3+}$, (bottom left) Δ-1-[Rh(GPB)$_2$phi]$^{5+}$, and (bottom right) Δ-1-[Rh(GEB)$_2$phi]$^{5+}$.

Experimental Section

Materials. Phosphoramidites, solid supports, and reagents for automated DNA synthesis were purchased from ABI and Glen Research.

(11) Pabo, C. O.; Sauer, R. T. *Annu. Rev. Biochem.* **1992**, *61*, 1053.
(12) Pavletich, N. L.; Pabo, C. O. *Science* **1991**, *252*, 809.
(13) Steitz, T. A. *Q. Rev. Biophys.* **1990**, *23*, 205.
(14) Terbrueggen, R. H.; Barton, J. K. *Biochemistry* **1995**, *34*, 8227.

Scheme 1. Synthetic Procedure Used for the Preparation 4-Guanidylmethyl-1,10-phenanthroline (**4**)

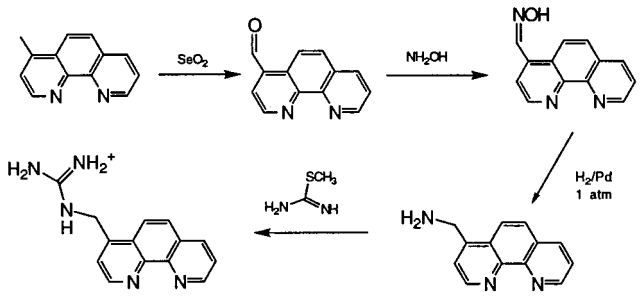

Oligonucleotides were synthesized via the phosphoramidite method[15] on an ABI 392 DNA−RNA synthesizer and purified by reverse-phase HPLC. DNA concentrations were determined using $\epsilon = 6600\ M^{-1}\ cm^{-1}$ per nucleotide at 260 nm. All restriction enzymes were purchased from New England Biolabs or Boehringer Mannheim. The concentrations of all rhodium complex solutions were determined by UV−visible spectroscopy using $\epsilon = 19\,400\ M^{-1}\ cm^{-1}$ at 358 nm.[16] [α-^{32}P]dATP and [γ-^{32}P]ATP were obtained from NEN-Dupont. A 330-base pair 3′-α-^{32}P-labeled *Acc*I/*Drd*I fragment of pBR322, a 140-base pair and 180-base pair 5′-γ-^{32}P- or 3′-α-^{32}P-labeled *Eco*RI/*Pvu*II fragment of pUC-18, and 636- and 190-base pair 5′-γ-^{32}P- or 3′-α-^{32}P-labeled *Eco*RI/*Pvu*II/*Eco*RV fragments of pB*R*322 were prepared by standard methods.[17]

Instrumentation. ^{1}H NMR spectra were recorded on a 300 MHz GE QE Plus spectrometer. Ultraviolet−visible (UV−vis) spectra were recorded on a Varian Cary 219 spectrophotometer. Circular dichroism studies were performed on a Jasco J-500a or a Jasco J-600 spectrometer. High-performance liquid chromatography (HPLC) was carried out on a Waters 600E system equipped with a Waters 484 tunable detector. A Vydac reverse phase protein and peptide C18 column was used for HPLC separations. A Chiralcel OD-R reverse phase HPLC column (Chiral Technologies) was used to inspect metal complex enantiomer distributions. Bulk enantiomer separations were performed on Sephadex SP C25 ion exchange beads (*vide infra*). All photocleavage experiments were performed using an Oriel Model 6140 1000 W Hg/Xe lamp fitted with a monochromator and a 300 nm cutoff filter. Gel electrophoresis experiments were quantified using a Molecular Dynamics phosphorimager and ImageQuant software. Chemicals were purchased from Aldrich Chemical Co. Mass spectra were recorded by the University of California at Riverside Mass Spectrometry Facility using electrospray ionization unless otherwise noted.

Synthesis of Metal Complexes. Ligand syntheses were carried out primarily as an adaption of methods described earlier for phenanthroline[18] and bipyridyl[19] funtionalizations. The strategies are illustrated in Schemes 1 and 2, and full details are provided as Supporting Information.

Bis(4-guanidylmethyl-1,10-phenanthroline)(phenanthrenequinone diimine)rhodium(III) Pentachloride, [Rh(MGP)$_2$phi]Cl$_5$ (19). $Rh(NO_3)_3{\cdot}xH_2O$ (30% Rh, 100 mg, 0.294 mmol) and **4** (168 mg, 0.588 mmol) were dissolved in 25 mL of 3:2 DMSO/H_2O. The pH of the solution was adjusted to 7 via addition of aqueous Na_2CO_3, and the solution was placed under an N_2 atmosphere. After heating to reflux for 12 h, 9,10-diaminophenanthrene (65 mg, 0.312 mmol) was added against a strong flow of nitrogen, and the reaction was refluxed for an additional 4 h. The pH was adjusted to 2 by addition of HCl (1.0 M). H_2O (50 mL) was added, and the solution was stirred vigorously open to the air for 24 h. The reaction was filtered through a frit, and the dark orange solution was evaporated to dryness. Purification by cation exchange chromatography (Sephadex SP C-25, 0.3 M $MgCl_2$) yielded [Rh(MGP)$_2$phi]Cl$_5$ as a mixture of 3 isomers (yield = 14%).

Scheme 2. Synthetic Procedure Used for the Preparation of 4-(2-Aminoethyl)-4′-methyl-2,2′-bipyridine (**8**), 4-(2-Guanidylethyl)-4′-methyl-2,2′-bipyridine (**9**), 4-(2-Amidoethyl)-4′-methyl-2,2′-bipyridine (**13**), 4-(3-Aminopropyl)-4′-methyl-2,2′-bipyridine (**17**), and 4-(3-Guanidylpropyl)-4′-methyl-2,2′-bipyridine (**18**)

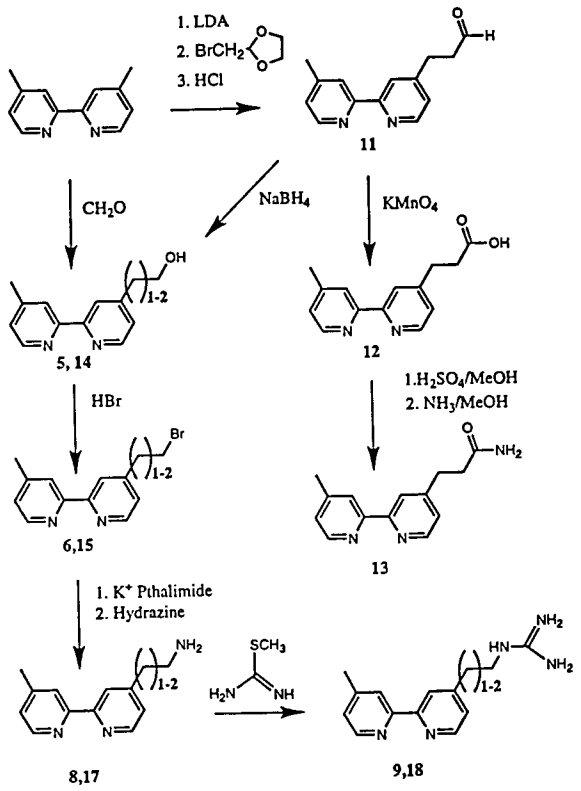

The enantiomers of each isomer were subsequently separated by cation exchange chromatography (Sephadex SP C-25/(+)-potassium antimonyl tartrate (0.15 M)). The isomers were loaded individually onto a resin (40 cm high) preequilibrated with 0.15 M potassium antimonyl tartrate. Over a 12 h period, enantiomer separation was obtained. The Λ-enantiomer of each isomer eluted first.

1-[Rh(MGP)$_2$phi]Cl$_5$. ^{1}H NMR(D_2O (pH 3), ppm): 5.05 (4H, dd), 7.4 (2H, t), 7.65 (4H, m), 7.85 (2H, d), 7.97 (2H, d), 8.03 (2H, d), 8.15 (2H, d), 8.35 (4H, dd), 8.75 (2H, d), 8.85 (2H, d). Calcd for $RhC_{42}H_{38}N_{12}$: 813.74. Found (FABMS *m*/*z*) 813 (M^+). UV−visible spectrum pH 5, H_2O-isobestic point at 366. Maxima at 380 and 272. CD (pH 5), (Δ) $\Delta\epsilon_{280} = -210\ cm^{-1}\ M^{-1}$, 259 (+), and 210 (−); (Λ) $\Delta\epsilon_{280} = +210$, 259 (−), and 210 (+) $cm^{-1}\ M^{-1}$.

2-[Rh(MGP)$_2$phi]Cl$_5$. ^{1}H NMR (D_2O (pH 3), ppm): 4.95 (4H, dd), 7.4 (2H, t), 7.6 (2H, d), 7.7 (2H, t), 7.85 (2H, d), 8.05 (4H, m), 8.15 (2H, d), 8.35 (4H, dd), 8.95 (2H, d), 9.0 (2H, d). Calcd for $RhC_{42}H_{38}N_{12}$: 813.74. Found (FABMS *m*/*z*) 813 (M^+). UV−visible spectrum pH 5, H_2O-isobestic point at 366. Maxima at 380 and 272. CD (pH 5), (Δ) peaks at 279 (−), 259 (+), and 210 (−).

3-[Rh(MGP)$_2$phi]Cl$_5$. ^{1}H NMR (D_2O (pH 3), ppm): 4.95 (2H, dd), 5.05 (2H, dd), 7.4 (2H, d), 7.55 (1H, d), 7.65 (3H, m), 7.75 (1H, d), 7.82 (1H, d), 7.95 (1H, d), 8.0 (3H, m), 8.1 (2H, d), 8.3 (4H, m), 8.75 (1H, d), 8.82 (1H, d), 8.9 (1H, d), 9.0 (1H, d). Calcd for $RhC_{42}H_{38}N_{12}$: 813.74. Found (FABMS *m*/*z*) 813 (M^+). UV−visible spectrum pH 5, H_2O-isobestic point at 366. Maxima at 380 and 272; CD (pH 5), (Δ) peaks at 279 (−), 259 (+), and 210 (−).

Bis(4-(2-amidoethyl)-4′-methyl-2,2′-bipyridine)(phenanthrenequinone diimine)rhodium(III) Trichloride, [Rh(amidoEB)$_2$phi]Cl$_3$ (20). $RhCl_3{\cdot}xH_2O$ (25 mg, 0.199 mmol) was dissolved in 5 mL of H_2O

(15) Caruthers, M. H.; Barone, A. D.; Beaucage, S. L.; Dodds, D. R.; Fisher, E. F.; McBride, L. J.; Matteucci, M.; Stabinsky, Z.; Tang, J.-Y. *Methods Enzymol.* **1987**, *154*, 287.
(16) Pyle, A. M.; Chiang, M. Y.; Barton, J. K. *Inorg. Chem.* **1990**, *29*, 4487.
(17) Maniatis, T.; Fritsch, E. F.; Sambrook, J. *Molecular Cloning*; Cold Spring Harbor Laboratory Press: Plainview, NY, 1982.
(18) Chandler, C. J.; Deady, L. W.; Reiss, J. A. *J. Heterocyclic Chem.* **1981**, *18*, 599.
(19) (a) Delle Ciana, L.; Hamachi, I.; Meyer, T. J. *J. Org. Chem.* **1989**, *54*, 1731−1735. (b) Belser, P.; Bernhard, S.; Guerig, U. *Tetrahedron*, **1996**, *52*, 2937.

and placed under a N_2 atmosphere. 9,10-Diaminophenanthrene (25 mg, 0.12 mmol) was added against a strong N_2 flow, and the reaction was heated to reflux for 2 h. **13** (59.0 mg, 0.245 mmol) was dissolved in 15 mL of DMF added via a syringe to the reaction mixture, and the resulting mixture was heated to reflux for 4 h. The pH was then adjusted to 1 by addition of 1.0 M HCl (1.0 M). A 50 mL amount of H_2O was added, and the solution was vigorously stirred under air contact for 24 h. The reaction mixture was filtered and concentrated by rotary evaporation. The isomers were separated by reverse phase HPLC (isocratic 84/16 H_2O with 0.1% trifluoroacetic acid/acetonitrile). Alternatively, a gradient of 100/0 H_2O/acetonitrile with 0.1% trifluoroacetic acid to 100% acetonitrile with 0.1% trifluoroacetic acid linearly over 1 h could be used. The isomers eluted in the same order as for **19**. Yield = 40%. Calcd for $RhC_{42}H_{40}N_8O_2$: 791.7. Found (*m*/*z* 789.5) (minus 2H).

1-[Rh(amidoEB)$_2$phi]Cl$_3$. ^{1}H NMR (D_2O (pH 3), ppm): 2.45 (6H, s), 2.65 (4H, t), 3.1 (4H, t), 7.3 (4H, s), 7.4 (2H, t), 7.55 (2H, d), 7.7 (2H, t), 8.1 (4H, t), 8.15 (2H, d), 8.4 (4H, d). UV−visible spectrum pH 5, peaks at 370, 311, 300 nm.

2-[Rh(amidoEB)$_2$phi]Cl$_3$. ^{1}H NMR (D_2O (pH 3), ppm): 2.5 (6H, s), 2.6 (4H, t), 3.05 (4H, t), 7.4 (6H, m), 7.5 (2H, d), 7.7 (2H, t), 8.1 (4H, t), 8.15 (2H, d), 8.4 (4H, d) UV−visible spectrum pH 5, peaks at 370, 311, 300 nm.

3-[Rh(amidoEB)$_2$phi]Cl$_3$. ^{1}H NMR (D_2O (pH 3), ppm) 2.4 (3H, s), 2.5 (3H, s), 2.6 (4H, m), 3.0 (2H, t), 3.1 (2H, t), 7.3 (2H, s), 7.4 (4H, t), 7.5 (1H, d), 7.55 (1H, s), 7.7 (2H, t), 8.1 (2H, s), 8.13 (2H, s), 8.17 (1H, d), 8.2 (1H, d), 8.35 (2H, s), 8.45 (2H, s). UV−visible spectrum pH 5, peaks at 370, 311, 300 nm.

Bis(4-(3-aminopropyl)-4′-methyl-2,2′-bipyridine)(phenanthrenequinone diimine)rhodium(III) Pentachloride, [Rh(aminoPB)$_2$phi]Cl$_5$ (21). The same synthethic procedure as for Rh(amidoEB)$_2$phi^{3+} (**20**) was used, but **17** was substituted as the bipyridine ligand. Yield = 25%. The isomers were separated by reverse phase HPLC (isocratic 85/15 H_2O with 0.1% trifluoroacetic acid/acetonitrile). The isomers eluted in the same order as for **19**. Calcd for $RhC_{42}H_{44}N_8$: 763.7. Found (ESI *m*/*z*) 761.5 (minus 2H).

1-[Rh(aminoPB)$_2$phi]Cl$_5$. ^{1}H NMR (D_2O (pH 3), ppm): 2.0 (4H, m), 2.45 (6H, s), 2.95 (8H, m), 7.3 (4H, m), 7.4 (2H, t), 7.6 (2H, d), 7.7 (2H, t), 8.1 (4H, t), 8.2 (2H, d), 8.4 (2H, s), 8.5 (2H, s). UV−visible spectrum pH 5, peaks at 370, 311, 300 nm.

2-[Rh(aminoPB)$_2$phi]Cl$_5$. ^{1}H NMR (D_2O (pH 3), ppm): 1.95 (4H, m), 2.5 (6H, s), 2.8 (4H, t), 2.9 (4H, t), 7.3 (4H, m), 7.4 (2H, t), 7.5 (2H, d), 7.65 (2H, t), 8.1 (4H, m), 8.2 (2H, d), 8.4 (2H, s), 8.45 (2H, s). UV−visible spectrum pH 5, peaks at 370, 311, 300 nm.

3-[Rh(aminoPB)$_2$phi]Cl$_5$. ^{1}H NMR (D_2O (pH 3), ppm): 1.95 (4H, m), 2.45 (3H, s), 2.5 (3H, s), 2.9−3.0 (6H, m), 7.25−7.45 (6H, m), 7.5 (1H, d), 7.6 (1H, d), 7.7 (2H, t), 8.1 (2H, m), 8.2 (2H, m), 8.25 (2H, d), 8.4 (2H, s), 8.45 (2H, s). UV−visible spectrum pH 5, H_2O− peaks at 370, 311, 300 nm.

Bis(4-(2-guanidylethyl)-4′-methyl-2,2′-bipyridine)(phenanthrenequinonediimine)rhodium(III) Pentachloride, [Rh(GEB)$_2$phi]Cl$_5$ (22). The same synthethic procedure as for **20** was used, but **9** was substituted as the bipyridine ligand and DMSO was used as a solvent instead of DMF. Yield = 20%. The stereoisomers and the enantiomers were separated simultaneously using cation exchange chromatography (Sephadex SP C-25/(+)-potassium antimonyl tartrate (0.15 M)). The separation was performed using the same procedure as was used for **19**, and the enantiomers eluted in the same order. Each enantiomer was further purified by reverse phase HPLC (isocratic 84/16 H_2O with 0.1% trifluoroacetic acid/acetonitrile). The isomers eluted in the same order as for **19**. Calcd for $RhC_{42}H_{44}N_{12}$: 819.7. Found (ESI *m*/*z*) 819.5.

1-[Rh(GEB)$_2$phi]Cl$_5$. ^{1}H NMR (D_2O (pH 3), ppm): 2.4 (3H, s), 2.9 (4H, t), 3.35 (4H, t), 7.3 (4H, s), 7.4 (2H, t), 7.55 (2H, d), 7.7 (2H, t), 8.1 (4H, t), 8.2 (2H, d), 8.35 (2H, s), 8.4 (2H, s). UV−visible spectrum pH 5, peaks at 370, 311, 300 nm. Circular dichroism (pH 5), (Δ) $\Delta\epsilon_{320} = -79$ cm^{-1} M^{-1}; (Λ) $\Delta\epsilon_{320} = +81$ cm^{-1} M^{-1}.

2-[Rh(GEB)$_2$phi]Cl$_5$. ^{1}H NMR (D_2O (pH 3), ppm): 2.5 (6H, s), 2.85 (4H, t), 3.3 (4H, t), 7.4 (6H, m), 7.55 (2H, d), 7.7 (3H, t), 8.1 (4H, t), 8.15 (2H, d), 8.4 (4H, d). UV−visible spectrum pH 5, peaks at 370, 311, 300 nm.

3-Rh(GEB)$_2$phi]Cl$_5$. ^{1}H NMR (D_2O (pH 3), ppm): 2.4 (3H, s), 2.5 (3H, s), 2.85 (2H, t), 2.95 (2H, t), 3.35 (4H, m), 7.3 (4H, m), 7.4 (2H, t), 7.5 (1H, d), 7.55 (1H, d), 7.7 (2H, t), 8.1 (4H, m), 8.17 (1H, d), 8.22 (1H, d), 8.35 (2H, d), 8.45 (2H, d). UV−visible spectrum pH 5, peaks at 370, 311, 300 nm.

Bis(4-(3-guanidylpropyl)-4′-methyl-2,2′-bipyridine)(phenanthrenequinone diimine)rhodium(III) Pentachloride, [Rh(GPB)$_2$phi]Cl$_5$ (23). The same synthethic procedure as for **20** was used, but **18** was substituted as the bipyridine ligand and DMSO was used as a solvent instead of DMF. Yield = 18%. The three isomers were separated by reverse phase HPLC (isocratic 84/16 H_2O with 0.1% trifluoroacetic acid/acetonitrile). The isomers eluted in the same order as for **19**. Calcd for $RhC_{44}H_{48}N_{12}$: 847.8. Found ESI *m*/*z* 847.6.

1-[Rh(GPB)$_2$phi]Cl$_5$. ^{1}H NMR (D_2O (pH 3), ppm): 1.8 (4H, m), 2.4 (6H, s), 2.8 (4H, t), 3.0 (4H, t), 7.3 (4H, s), 7.4 (2H, t), 7.55 (2H, d), 7.7 (2H, t), 8.1 (4H, t), 8.2 (2H, d), 8.35 (2H, s), 8.4 (2H, s). UV−visible spectrum pH 5, peaks at 370, 311, 300 nm.

2-[Rh(GPB)$_2$phi]Cl$_5$. ^{1}H NMR (D_2O (pH 3), ppm): 1.75 (4H, m), 2.5 (6H, s), 2.75 (4H, t), 2.95 (4H, t), 7.3−7.4 (6H, m), 7.5 (2H, d), 7.7 (2H, t), 8.1−8.2 (6H, m), 8.35 (2H, s), 8.4 (2H, s). UV−visible spectrum pH 5, peaks at 370, 311, 300 nm.

Photocleavage Reactions on 5′ and 3′-^{32}P Restriction Fragments. The ^{32}P end-labeled restriction fragment and rhodium complexes were incubated together in a 1.7 mL siliconized Eppendorf tube at 23 °C for 5 min prior to irradiation with 313 nm light for 8 min. The DNA/Rh ratio was maintained at 50 nucleotides:1 by addition of unlabeled calf thymus DNA (Pharmacia) in 20 μL irradiation reactions (10 mM sodium cacodylate, 40 mM NaCl, pH 7.0). Samples were frozen on dry ice immediately after irradiation and lyophilized to dryness. The pellet was resuspended in 15 μL of denaturing gel loading dye, and 3 μL was loaded onto an 8% denaturing polyacrylamide gel and electrophoresed at 90 W (@2000 V) for 90 min. The gel was transferred to paper and dried prior to being analyzed using a phosphorimager (Molecular Dynamics).

Photocleavage Reactions on 5′-^{32}P-End-Labeled Oligonucleotides. A series of oligonucleotides, (**A1/A2**) 5′-GTAGGTGAACCTCGGACGATCTCAACATCTGTTAATCTTGGTTTCTAAGGT-TCTTCCGCTTCAGAAGTTCACAGGTGA-3′, (**B1/B2**) 5′-CTGTAGGTGGTCGACA-ATCGATGCCCGGGACACGTGACTTCTGACTTCAGACTGCAGACACGTGACATCTGAGGTCAC-3′, (**C1/C2**) 5′-TAGTTCGGCGTCGACGCTCGAGACTTCA-GAGTCTACTCTCTAGTGTGCAGAATCTATGTTCTAACCGGAATC-3′, and (**D1/D2**) 5′-ACTGGCCTCATCTGCTCTTCAGCAGCTGC TGCAGGTCTAGGGCAT-3′, and their complements were synthesized on solid supports using phosphoramidite chemistry[15] for use in determining the sequence-specificity of Δ-1-[Rh(MGP)$_2$phi]$^{5+}$ and Δ-1-[Rh(GEB)$_2$phi]$^{5+}$. The oligonucleotides (both strands) were 5′-^{32}P labeled by standard protocols.[17] Each oligonucleotide strand was annealed with a slight excess of its cold complement by incubation at 90 °C for 4 min followed by cooling to 23 °C over a 1 h period. The double-stranded oligonucleotides and the different rhodium complexes were incubated together at 23 °C for 5 min prior to irradiation with 313 nm light for 10 min. The DNA-(nucleotides)/Rh ratio was 100:1 with 20 μL irradiation reactions (10 mM sodium cacodylate, 40 mM NaCl, pH 7). Samples were frozen on dry ice immediately after irradiation, and lyophilized to dryness. The pellet was resuspended in 15 μL of denaturing gel loading dye, and 3 μL was loaded onto an 8% denaturing polyacrylamide gel and electrophoresed at 90 W (@2000 V) for 90 min. The gel was transferred to paper and dried prior to being analyzed using a phosphorimager (Molecular Dynamics).

Binding Constants for Δ- and Λ-1-[Rh(MGP)$_2$phi]$^{5+}$. The oligonucleotide 5′-CTC***CATATG***GAGACTC***CATCTG***GAGACTCTAGAGAGACTCTTGC-AAGAGACTCCCATGGGAG-3′, where the italicized sequences are the recognition sites for Λ- and Δ-1-[Rh(MGP)$_2$phi]$^{5+}$, and its complement were synthesized, labeled, and annealed as above. Binding constants were determined by conducting photocleavage experiments while holding the DNA template-to-rhodium ratio constant at 2:1 for the Λ enantiomer and at 10:1 for the Δ enantiomer.[20] Samples containing DNA template concentrations from 1 nM to 10 μM were irradiated, and the amount of photocleavage at

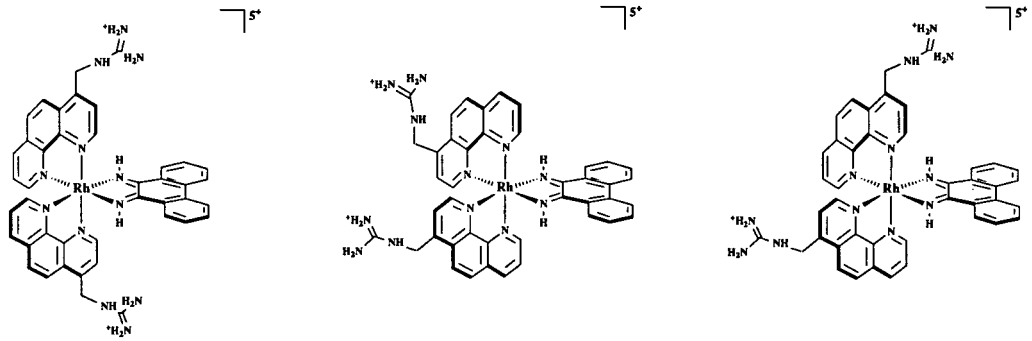

Figure 2. Three diastereomers of $[Rh(MGP)_2phi]^{5+}$. Δ-1-$[Rh(MGP)_2phi]^{5+}$ (left) the symmetric diastereomer which has both arms directed toward the DNA when the phi ligand is intercalated; Δ-3-$[Rh(MGP)_2phi]^{5+}$ (right) the asymmetric diastereomer; Δ-2-$[Rh(MGP)_2phi]^{5+}$ (center) the symmetric diastereomer which has both arms directed away from the DNA when the phi ligand is intercalated.

the recognition sequence for each complex determined by phosphorimager analysis. The resulting data were then fit to the following model:

$$\text{DNA} + \text{Rh} \overset{K_b}{\leftrightarrow} \text{DNA·Rh} \overset{k_c}{\rightarrow} \text{cleaved DNA}$$

where K_b is the binding constant of the rhodium for its target DNA site and k_c is the kinetic constant for photocleavage by bound rhodium. The data were fit to the model using Sigma Plot on a Windows 95-based PC.[21]

Results

Synthesis and Characterization of Metal Complexes. The synthetic routes to the functionalized ligands are described in Schemes 1 and 2. Variations on previously described procedures[18,19] for modifying bipyridyl and phenanthroline ligands were employed in routes to the final ligands prepared. For the first time, we have isolated phenanthroline and bipyridine derivatives containing appended guanidinium moieties. These guanidinium derivatives are prepared from the amino phenanthroline and bipyridine compounds via the use of 2-methyl-2-thiopseudourea. Importantly, it is necessary to add Zn^{2+} to the reaction mixture in order to stabilize the guanidinium ligands; otherwise the ligands rapidly decompose, even under an inert atmosphere.

New methodologies for the synthesis of $[Rh(phen)_2phi]^{3+}$ and $[Rh(bpy)_2phi]^{3+}$ derivatives were also developed. These procedures differ significantly from previously described methods.[3,5b] Previous methods involved multistep procedures which employed harsh conditions and gave low overall yields. For example, $[Rh(phen)_2phi]^{3+}$ and $[Rh(bpy)_2phi]^{3+}$ derivatives are usually prepared from the corresponding bisphen dichloro or bisbpy dichloro intermediates, $[Rh(phen\text{-}x)_2Cl_2]Cl$ or $[Rh(bpy\text{-}x)_2Cl_2]Cl$. The dichloro complexes are then converted to the diaquo complexes by using silver salts or base. The resulting diaquo complex is then reacted with 9,10-diaminophenanthrene and air oxidized to yield the desired phi complexes of rhodium(III). Unfortunately, many functionalities, such as amino and guanidinium functionalities, are incompatible with the use of the silver salts. Thus a new method for the synthesis of $Rh(phen)_2phi^{3+}$ derivatives was needed. Here we employ instead a one-pot synthesis of the coordination complexes. This procedure allows for the preparation of rhodium complexes which possess sensitive functionalities, such as the amino and guanidinium moieties.

Separation of Isomers of Metal Complexes. Due to the asymmetric nature of the bipyridine and phenanthroline ligands used, the derivatives of $[Rh(phen)_2phi]Cl_3$ and $[Rh(bpy)_2phi]Cl_3$ were generated as a mixture of three isomers. For example, $[Rh(MGP)_2phi]Cl_5$ was obtained as a 1:2:1 mixture of 3 isomers, as expected statistically. The configurational isomers were separated by reverse-phase HPLC (isocratic conditions: 86/14 H_2O with 0.1% trifluoroacetic acid/acetonitrile). Figure 2 shows the structures of the three isomers of $[Rh(MGP)_2phi]^{5+}$. The first isomer which elutes via HPLC is the C_2-symmetric isomer with both methyl guanidinium functionalities disposed over the phi ligand, 1-$[Rh(MGP)_2phi]Cl_5$. The second isomer which elutes is assigned as the asymmetrical isomer, 3-$[Rh(MGP)_2phi]Cl_5$. The third isomer is the C_2 symmetric isomer with both functionalities positioned away from the phi ligand, 2-$[Rh(MGP)_2phi]Cl_5$.

Structural assignments of the two symmetric isomers are made by NMR comparison with $[Rh(phen)_2phi]Cl_3$. The NMR assignments[6] for $[Rh(phen)_2phi]Cl_3$ show that the C2 (also C9 for the underivatized ligand) proton of the ancillary phenanthroline ring is shifted downfield by 0.4 ppm when it is pointed toward the phi ligand rather than toward the other phenanthroline ligand. This downfield shift has to do with the difference in spatial orientation of the π-system of the phenanthroline and phi ligands relative to the C3 proton of the other phenanthroline. The phi ligand is extended away from the metal center relative to the phenanthroline ligand, and as a result, the C2 hydrogen projects further into the ring currents of the phenanthroline ligand and is shielded to a greater extent. This trend holds true in the derivatized $[Rh(phen)_2phi]Cl_3$ complexes as well and makes possible the assignment of positional isomers. Differentiation between H2 and H3 and their counterparts H8 and H9 are possible in functionalized ligands because H2 and H3 have NOEs only between themselves. It is then possible by inspection of their NMRs to establish whether they were directed toward or away from the phi ligand. Similar reasoning was used in assigning the isomers of the bipyridyl derivatives.

Purification of Enantiomers. Each isomer of $[Rh(MGP)_2phi]Cl_5$ exists as an equal mixture of two enantiomers. Previous methods for the purification of enantiomers of $[Rh(phen)_2phi]^{3+}$ have relied on the use cation exchange chromatography with tris(L-cysteinylsulfinato)cobaltate(III) as a chiral eluant.[3] However, attempts to resolve the guanidinium functionalized isomers using this procedure were unsuccessful. It was subsequently discovered that each isomer of $[Rh(MGP)_2phi]Cl_5$ could be separated on a chiral HPLC column into its enantiomers. It was possible to obtain baseline resolution between the Δ and Λ enantiomers of $[Rh(MGP)_2phi]Cl_5$ on a reverse phase cellulose tris(3,5-dimethylphenyl carbamate) support.[22] This chiral chromatographic method could, in addition, be used to separate the enantiomers of a variety of rhodium bis(phenanthroline) phi

(20) Singleton, S. F.; Dervan, P. B. *J. Am. Chem. Soc.* **1992**, *114*, 6957.
(21) Jackson, B. A.; Hastings, C. A.; Johann, T. J.; Hudson, B. P.; Barton, J. K. Manuscript in preparation.

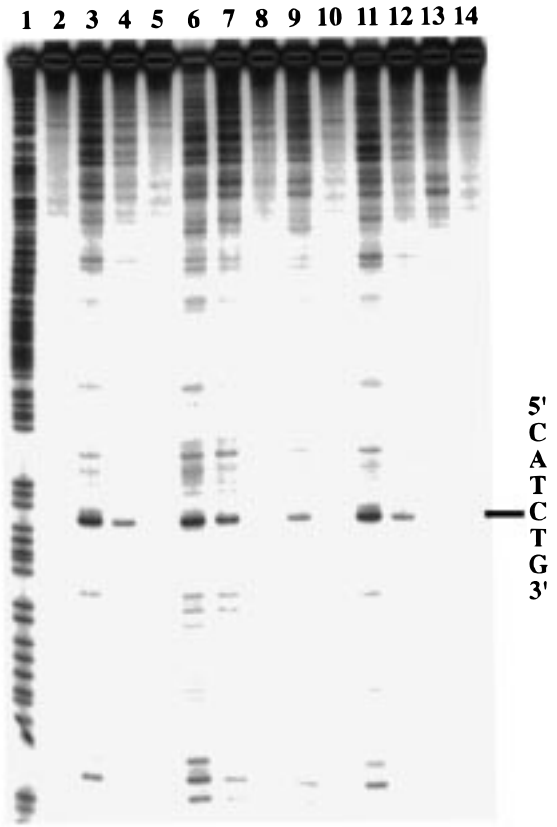

Figure 3. Photocleavage with racemic mixtures of $[Rh(phen)_2phi]^{3+}$, $[Rh(MGP)_2phi]^{5+}$, $[Rh(GEB)_2phi]^{5+}$, $[Rh(GPB)_2phi]^{5+}$, $[Rh(amidoEB)_2phi]^{3+}$, and $[Rh(aminoPB)_2phi]^{5+}$ on a 3′-^{32}P-labeled 330-bp restriction fragment. Lane 1, Maxam−Gilbert A+G reaction; lane 2, 0.1 μM *rac*-1-$[Rh(phen)_2phi]^{5+}$; lane 3, 0.1 μM *rac*-1-$[Rh(MGP)_2phi]^{5+}$; lane 4, 0.1 μM *rac*-1-$[Rh(GEB)_2phi]^{5+}$; lane 5, 0.1 μM *rac*-1-$[Rh(GPB)_2phi]^{5+}$; lane 6, 0.1 μM *rac*-1-$[Rh(AEB)_2phi]^{3+}$; lane 7, 0.1 μM *rac*-1-$[Rh(aminoPB)_2phi]^{5+}$; lane 8, 0.1 μM Δ-1-$[Rh(MGP)_2phi]^{5+}$; lane 9, 0.1 μM Δ-1-$[Rh(GEB)_2phi]^{5+}$; lane 10, 0.1 μM Λ-1-$[Rh(MGP)_2phi]^{5+}$; lane 11, 0.1 μM Λ-1-$[Rh(GEB)_2phi]^{5+}$; lane 12, DNA only.

derivatives. We subsequently observed that all 6 isomers (3 geometrical isomers, each with 2 enantiomers) of $[Rh(MGP)_2phi]Cl_5$ and $[Rh(GEB)_2phi]Cl_5$ could be resolved simultaneously by cation exchange chromatography using (+)-potassium antimonyl tartrate as a chiral eluant. For these isomers, the assignments of absolute configuration were made spectroscopically by comparison to $[Rh(phen)_2phi]^{3+}$,[3] since functionalization leaves the primary phenanthroline absorption band and resulting circular dichroism unperturbed.

DNA Photocleavage by Functionalized Rhodium Complexes. In Figure 3, photocleavage by racemic mixtures of 1-$[Rh(aminoPB)_2phi]^{5+}$, 1-$[Rh(amidoEB)_2phi]^{3+}$,1-$[Rh(MGP)_2phi]^{5+}$, 1-$[Rh(GEB)_2phi]^{5+}$, 1-$[Rh(GPB)_2phi]^{5+}$, and $[Rh(phen)_2phi]^{3+}$ are directly compared on a 3′-^{32}P-end-labeled 330 bp DNA restriction fragment. The general pattern of DNA damage for all five complexes is remarkably similar. Of particular note are two strong sites which are targeted: 5′-CAT***C***TG-3′, in which cleavage is evident at the italicized C, and 5′-CA***TA***TG-3′, in which cleavage is apparent at two sites, the central italicized T and A. The former site corresponds to the strongest site targeted by Δ-1-$[Rh(MGP)_2phi]^{5+}$ (lane 8), while the latter represents that specifically recognized by Λ-1-$[Rh(MGP)_2phi]^{5+}$ (lane 10). These two sites differ by a single nucleotide. All of the Δ-isomers of the functionalized complexes appear to cleave 5′-CATCTG-3′, albeit to differing extents. Specific recognition of 5′-CATATG-3′ is more sensitive to the presence of the functional group placement; specific recognition is apparent only with Λ-1-$[Rh(MGP)_2phi]^{5+}$ and Λ-1-$[Rh(GEB)_2phi]^{5+}$.[23]

(22) Enantiomers were separated on a Chiralcel OD-R reverse phase HPLC column (Chiral Technologies). The eluant was acetonitrile/aqueous phase (pH 2, 0.5 M $HClO_4/NaClO_4$. The best separation was obtained under isocratic conditions at 78/22 acetonitrile/aqueous phase.

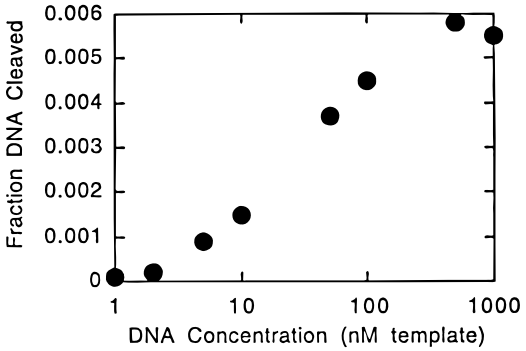

Figure 4. Plot of photocleavage data from experiments determining quantitative affinity constants for 1-Δ-$[Rh(MGP)_2phi]^{5+}$ binding to 5′-CATCTG-3′. Conditions are described in the Experimental Section. In short, the rhodium/DNA template ratio was held constant at 1:10 while the absolute concentrations of these reagents were varied over 4 orders of magnitude. The resulting photocleavage data was then fit as described in the Experimental Section to yield an affinity constant of $5(\pm1) \times 10^7\ M^{-1}$.

Site Affinity of Λ- and Δ-1-$[Rh(MGP)_2phi]^{5+}$. To determine the affinity of the Δ and Λ enantiomers of 1-$Rh(MGP)_2phi^{5+}$ for their respective consensus sequences, photocleavage experiments as a function of concentration were carried out on an oligonucleotide containing these sites. Figure 4 shows a photocleavage titration for Δ-1-$[Rh(MGP)_2phi]^{5+}$. The binding affinities of the enantiomers for their respective sites are comparable. On the oligomer prepared, Λ-1-$[Rh(MGP)_2phi]^{5+}$ shows an affinity of 1.1 (+0.5) $\times 10^8\ M^{-1}$ for 5′-CATATG-3′, while Δ-1-$[Rh(MGP)_2phi]^{5+}$ displays an affinity of 5 (±2) $\times 10^7\ M^{-1}$ for 5′-CATCTG-3′. However, even at concentrations 2 orders of magnitude higher, no cleavage by the Λ-isomer is evident at 5′-CATCTG-3′, the recognition site for the Δ-isomer, nor does the Δ-isomer show cleavage at 5′-CATATG-3′. It is interesting that despite the higher intensity of photocleavage for the Δ-isomer, it is the Λ-isomer which displays the higher site-affinity; this difference must reflect the differing photocleavage efficiencies for the two isomers in their respective sites, likely an effect of their differing orientations within their sites.

Cleavage on an oligonucleotide duplex containing variations within the target sequence 5′-CATCTG-3′ was examined to evaluate how DNA sequence variations affect recognition by Δ-1-$[Rh(MGP)_2phi]^{5+}$. Based upon extensive screening of photocleavage by Δ-1-$[Rh(MGP)_2phi]^{5+}$ on DNA restriction fragments, sites were designed to contain a central 5′-TC-3′ step, with flanking base pairs varied symmetrically. An analogous study[14] had been performed earlier for Λ-1-$[Rh(MGP)_2phi]^{5+}$ and the results for both isomers are summarized in Table 1. The heirarchy for outer bases recognized is quite similar for both isomers. Recognition is most sensitive to variations in the central bases of the site. Indeed, in the case of Λ-1-$[Rh(MGP)_2phi]^{5+}$, no cleavage at all is detectable for the site 5′-CACGTG-3′.

DNA Photocleavage by $[Rh(amidoEB)_2phi]^{3+}$ and $[Rh(aminoPB)_2phi]^{5+}$. The intensity of photocleavage by racemic

(23) Note that there is a three-band pattern at a site neighboring 5′-CATATG-3′.

Table 1. Relative Intensities of Photocleavage at Various DNA Sites by Phi Complexes of Rhodium (Adapted from Ref 14)[a−c]

site	Λ-1-Rh(MGP)$_2$phi^{5+}	site	Δ-1-Rh(MGP)$_2$phi^{5+}	Δ-1-Rh(GEB)$_2$phi^{5+}
5′-CATATG-3′	100	5′-CATCTG-3′	100	44
5′-CACGTG-3′	0	5′-CAGCTG-3′	10	5
5′-TATATA−3′	73	5′-TATCTA−3′	75	27
5′-GATATC−3′	67	5′-GATCTC−3′	68	49
5′-CTTAAG-3′	16	5′−CTTCAG-3′	48	17

[a] Photocleavage reactions were carried out with 5′-labeled 76mer (Λ-1-[Rh(MGP)$_2$phi]$^{5+}$) and 77mer (Δ-1-[Rh(MGP)$_2$phi]$^{5+}$and Δ-1-[Rh(GEB)$_2$phi]$^{5+}$) oligonucleotides containing all five sites. DNA and rhodium concentrations were 10 μM base pairs and 0.1 μM, respectively, in 10 mM sodium cacodylate, 40 mM NaCl, pH 7.0. [b] Photocleavage intensities were calculated by analyzing cleavage bands on a polyacrylamide gel via phosphorimagery. The strongest site of photocleavage was normalized to 100, and all other intensities are reported relative to it. [c] The estimated error for reported values is ±10%.

1-[Rh(amidoEB)$_2$phi]$^{5+}$ and 1-[Rh(aminoPB)$_2$phi]$^{3+}$ was directly compared with that by 1-[Rh(MGP)$_2$phi]$^{5+}$ and [Rh(phen)$_2$phi]$^{3+}$ on a 3′-^{32}P-end-labeled 330-bp restriction fragment. As shown in Figure 3, the strongest site for 1-[Rh(aminoPB)$_2$phi]$^{5+}$ (lane 7) and 1-[Rh(amidoEB)$_2$phi]$^{3+}$ (lane 6) is 5′-CATCTG-3′, the consensus site for Δ-1-[Rh(MGP)$_2$phi]$^{5+}$ (lane 8). The overall intensity of photocleavage by 1-[Rh(aminoPB)$_2$phi]$^{5+}$, is greater than that of 1-[Rh(MGP)$_2$phi]$^{5+}$ (lane 3); however, 1-[Rh(aminoPB)$_2$phi]$^{5+}$ is somewhat less specific than 1-[Rh(MGP)$_2$phi]$^{5+}$. 1-[Rh(amidoEB)$_2$phi]$^{5+}$ most closely resembles [Rh(phen)$_2$phi]$^{3+}$ in both affinity and specificity; no new recognition specificity is seen on this DNA fragment for the amido-functionalized complex. It is also evident that the aminopropyl functionality does not provide a simple replacement for the guanidinium functionality in directing recognition. These observations are further supported in photocleavage experiments at a range of concentrations on different DNA restriction fragments (data not shown).

DNA photocleavage by the different isomers of [Rh(amidoEB)$_2$phi]$^{3+}$ and [Rh(aminoPB)$_2$phi]$^{3+}$ is also shown as a function of concentration on a 3′-^{32}P-end-labeled 636-bp DNA restriction fragment (Figure 5). The presence of neither functionality affects the overall photocleavage behavior. Photocleavage experiments at low rhodium concentration allow one to distinguish the presence of any sites with particularly high affinity. One may first contrast characteristics of geometric isomers with functional groups positioned toward (1) or away from (2) the intercalating phi ligand. Comparison of the photocleavage pattern of 1-[Rh(amidoEB)$_2$phi]$^{3+}$ (lanes 1−3) with that of 2-[Rh(amidoEB)$_2$phi]$^{3+}$ (lanes 4−6) reveals little difference in the sequence specificity of the two molecules. The overall pattern of cleavage is essentially the same, as is the intensity of cleavage at high concentrations. One noticeable difference is that 1-[Rh(amidoEB)$_2$phi]$^{3+}$ shows an increase in photocleavage intensity at low concentrations compared to 2-[Rh(amidoEB)$_2$phi]$^{3+}$ (lane 3 versus lane 6). This small difference provides the only indication of any DNA interaction of the pendant amide functionality but likely reflects a small difference in overall binding affinity rather than site-selectivity.

Figure 5 also presents the comparison of DNA photocleavage by 1-[Rh(aminoPB)$_2$phi]$^{5+}$ (lanes 7−9) with that of 2-[Rh(aminoPB)$_2$phi]$^{5+}$ (lanes 10−12). At high concentrations, both isomers containing the aminopropyl functionality display a photocleavage pattern which is somewhat more intense than that of the amido complex. Direct comparison of 1-[Rh(aminoPB)$_2$phi]$^{5+}$ with 2-[Rh(aminoPB)$_2$phi]$^{5+}$ shows some obvious differences, however. The overall cleavage intensity of the isomer with both arms directed away from the DNA, 2-[Rh(aminoPB)$_2$phi]$^{5+}$, shows more intense photocleavage than 1-[Rh(aminoPB)$_2$phi]$^{5+}$. This indicates a higher affinity for DNA or higher photocleavage efficiency for this isomer. 1-[Rh(aminoPB)$_2$phi]$^{5+}$ also shows some sites in which the photocleavage intensity is markedly lowered compared to 2-[Rh(aminoPB)$_2$phi]$^{5+}$. These sites, indicated by asterisks in Figure 5, are 5′-CA***T***GAC-3′ and 5′-GA***C***GTC-3′ with photocleavage at the bold italicized bases.

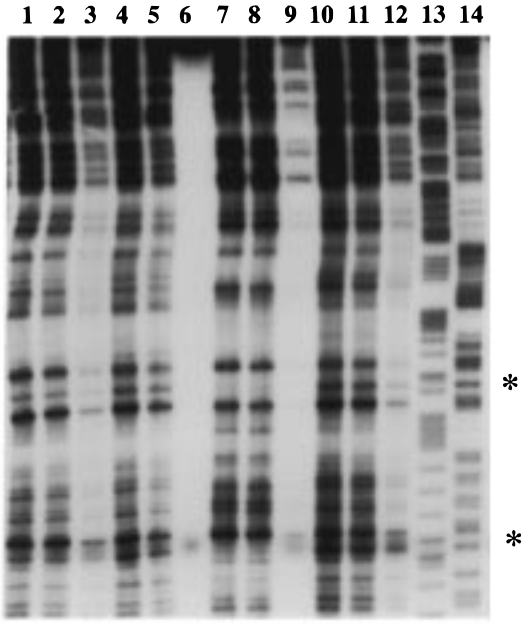

Figure 5. Photocleavage with the racemates of the different diastereomers of [Rh(aminoPB)$_2$phi]$^{5+}$ and [Rh(amidoEB)$_2$phi]$^{3+}$ on a 3′-^{32}P-end-labeled 636-bp restriction fragment. Lane 1, 1.0 μM *rac*-1-[Rh(amidoEB)$_2$phi]$^{5+}$; lane 2, 0.1 μM *rac*-1-[Rh(amidoEB)$_2$phi]$^{5+}$; lane 3, 0.01 μM *rac*-1-[Rh(amidoEB)$_2$phi]$^{5+}$; lane 4, 1.0 μM *rac*-2-[Rh(amidoEB)$_2$phi]$^{5+}$; lane 5, 0.1 μM *rac*-2-[Rh(amidoEB)$_2$phi]$^{5+}$; lane 6, 0.01 μM *rac*-2-[Rh(amidoEB)$_2$phi]$^{5+}$; lane 7, 1.0 μM *rac*-1-[Rh(aminoPB)$_2$phi]$^{5+}$; lane 8, 0.1 μM *rac*-1-[Rh(aminoPB)$_2$phi]$^{5+}$; lane 9, 0.01 μM *rac*-1-[Rh(aminoPB)$_2$phi]$^{5+}$; lane 10, 1.0 μM *rac*-2-[Rh(aminoPB)$_2$phi]$^{5+}$; lane 11, 0.1 μM *rac*-2-[Rh(aminoPB)$_2$phi]$^{5+}$; lane 12, 0.01 μM *rac*-2-[Rh(aminoPB)$_2$phi]$^{5+}$; lane 13, Maxam−Gilbert A+G reaction; lane 14, Maxam−Gilbert C+T reaction.

Photocleavage with [Rh(GEB)$_2$phi]$^{5+}$ and [Rh(GPB)$_2$phi]$^{5+}$. To explore the effect of variation in the length of the linker arm between the metal complex and the guanidinium moiety, the DNA photocleavage properties of [Rh(GEB)$_2$phi]$^{5+}$ and [Rh(GPB)$_2$phi]$^{5+}$ may be compared. Both of these complexes have the same general shape as [Rh(MGP)$_2$phi]$^{5+}$, but the linker arm between the bipyridyl ligand and the guanidinium is varied from methyl to ethyl to propyl.

As is evident in Figure 6, the intensity of photocleavage by 1-[Rh(GEB)$_2$phi]$^{5+}$ does vary depending on the spatial positioning of the ethyl guanidinium moiety. This is evident by comparing the photocleavage of 1-[Rh(GEB)$_2$phi]$^{5+}$ (lanes 3 and 4) with 2-[Rh(GEB)$_2$phi]$^{5+}$ (lanes 5 and 6). The strongest site of reaction for both isomers is 5′-CATCTG-3′, however cleavage by 1-[Rh(GEB)$_2$phi]$^{5+}$ is stronger at low concentrations

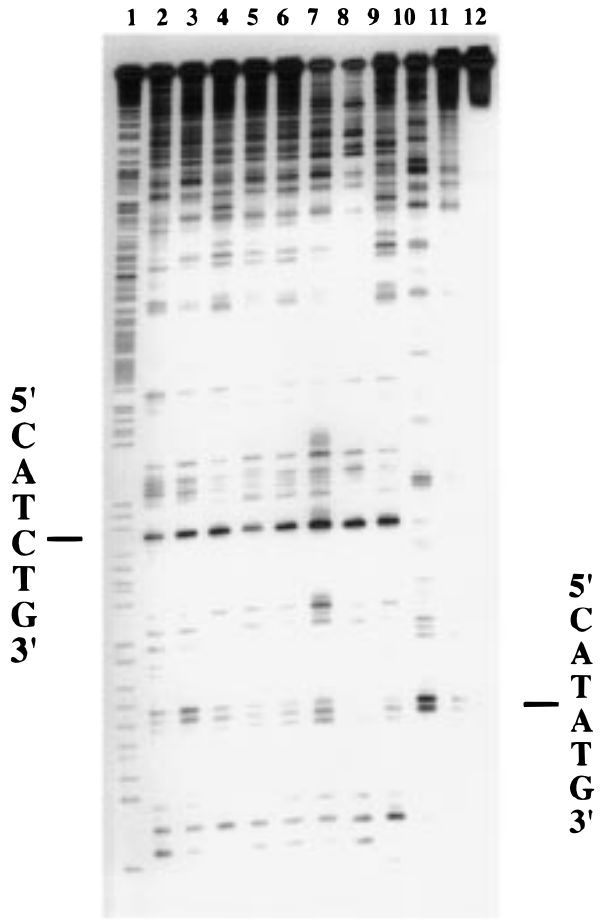

Figure 6. Photocleavage with $[Rh(GEB)_2phi]^{5+}$ and $[Rh(GPB)_2phi]^{5+}$ on a 3′-^{32}P-labeled 330-bp restriction fragment. Lane 1, Maxam−Gilbert A+G reaction; lane 2, DNA only; lane 3, 0.1 μM *rac*-1-$[Rh(GEB)_2phi]^{5+}$; lane 4, 0.01 μM *rac*-1-$[Rh(GEB)_2phi]^{5+}$; lane 5, 0.01 μM *rac*-2-$[Rh(GEB)_2phi]^{5+}$; lane 6, 0.1 μM *rac*-2-$[Rh(GEB)_2phi]^{5+}$; lane 7, 0.1 μM *rac*-1-$[Rh(GPB)_2phi]^{5+}$; lane 8, 0.01 μM *rac*-1-$[Rh(GPB)_2phi]^{5+}$; lane 9, 0.1 μM *rac*-2-$[Rh(GPB)_2phi]^{5+}$; lane 10, 0.01 μM *rac*-2-$[Rh(GPB)_2phi]^{5+}$; lane 11, 0.1 μM Δ-1-$[Rh(GEB)_2phi]^{5+}$; lane 12, 0.01 μM Δ-1-$[Rh(GEB)_2phi]^{5+}$; lane 13, 0.1 μM Λ-1-$[Rh(GEB)_2phi]^{5+}$; lane 14, 0.01 μM Λ-1-$[Rh(GEB)_2phi]^{5+}$.

(lane 4 versus lane 5). Photocleavage with the guanidylpropyl complex, 1-$[Rh(GPB)_2phi]^{5+}$, shows that the photocleavage intensity for this complex also varies with stereochemistry. Photocleavage by 1-$[Rh(GPB)_2phi]^{5+}$ (lane 7) is significantly more intense than the photocleavage seen by 2-$[Rh(GPB)_2phi]^{5+}$ (lane 9). Both isomers however show less intense photocleavage compared to isomers of $[Rh(GEB)_2phi]^{5+}$.

The direct comparison between the enantiomers of 1-$[Rh(MGP)_2phi]^{5+}$ and 1-$[Rh(GEB)_2phi]^{5+}$ is given in Figure 3. As for $[Rh(MGP)_2phi]^{5+}$, DNA photocleavage by $[Rh(GEB)_2phi]^{5+}$ is isomer-specific and enantiomer-specific. Comparison of the Δ-enantiomers of each (lanes 8 and 9) shows that, as above, the overall pattern of photocleavage is very similar for both complexes. Interestingly, the strongest site of cleavage for both Δ-1-$[Rh(MGP)_2phi]^{5+}$ and Δ-1-$[Rh(GEB)_2phi]^{5+}$ is 5′-CATCTG-3′. Comparison of Λ-1-$[Rh(MGP)_2phi]^{5+}$ and Λ-1-$[Rh(GEB)_2phi]^{5+}$ shows that while both complexes target 5′-CATATG-3′, Λ-1-$[Rh(MGP)_2phi]^{5+}$ does so with significantly greater intensity.

Given the similarities between $[Rh(GEB)_2phi]^{5+}$ and $[Rh(MGP)_2phi]^{5+}$, we also examined the hierarchy of sites recognized by this complex (Table 1). The consensus recognition site for Δ-1-$[Rh(GEB)_2phi]^{5+}$ was determined using the same oligonucleotides as for Δ-1-$[Rh(MGP)_2phi]^{5+}$. It is interesting that the hierarchy for recognition differs somewhat compared to Δ-1-$[Rh(MGP)_2phi]^{5+}$. The strongest site of reaction for Δ-1-$[Rh(GEB)_2phi]^{5+}$ is found to be 5′-GATCTC-3′, with photocleavage at 5′-CATCTG-3′ slightly less intense. As seen with Δ-1-$[Rh(MGP)_2phi]^{5+}$, photocleavage by Δ-1-$[Rh(GEB)_2phi]^{5+}$ is also evident primarily on one strand.[24]

Discussion

Several different variations on the parent complexes $[Rh(bpy)_2phi]^{3+}$ and $[Rh(phen)_2phi]^{3+}$ which contain pendant guanidinium, amine, or amido functionalities have been prepared. By positioning these functionalities with different aliphatic linkers onto the ancillary ligands and with the formation of different geometric and stereoisomers, a family of molecules may be screened with respect to elements of DNA recognition. The DNA binding and photocleavage properties of these complexes may be compared to determine how these variations affect DNA binding specificity and affinity.

Synthesis and Characterization of Metal Complexes. Here we have described the first synthesis of phenanthroline and bipyridine ligands containing appended guanidinium moieties and their application in constructing coordination complexes. Coordination to rhodium furthermore required the development of new methodologies. Previous methods involved multistep procedures which employed conditions incompatible with these functionalities. Instead, a one-pot synthesis of the coordination complexes was developed (Scheme 3). This procedure allows for the preparation of novel rhodium complexes which possess sensitive organic functionalities, such as the amino and guanidinium moieties.

Site-Specific Targeting of DNA by Δ-1- and Λ-1-$[Rh(MGP)_2phi]^{5+}$. Both Δ-1- and Λ-1-$[Rh(MGP)_2phi]^{5+}$ bind to their respective DNA sites with high affinity. The specific binding constants for these complexes are approximately 2 orders of magnitude higher than those of the parent complex $[Rh(phen)_2phi]^{3+}$ [3,4] and approximately 4 orders of magnitude higher than tris(phenanthroline)metal complexes.[25] Metallointercalators may therefore be constructed easily which bind DNA with high affinity. In a stepwise fashion, DNA-binding metal complexes have been prepared containing a high-affinity intercalating unit, the phi ligand, to orient the octahedral metal complex with respect to the DNA helix, and functionalized ancillary ligands to establish an ensemble of noncovalent contacts in the DNA groove.

The similarities and differences in targeting by these two enantiomers are useful to consider as lessons in new design strategies. Site-specific targeting by these complexes is highly enantioselective. No overlap in sites targeted is apparent over at least 3 orders of magnitude in concentration. This difference in recognition quite simply underscores the importance of stereochemical control over the placement of functional groups for site-specific design.

First we consider Λ-1-$[Rh(MGP)_2phi]^{5+}$ and the hierarchy of sites which it targets. As described earlier,[14] Λ-1-$[Rh(MGP)_2phi]^{5+}$ targets 5′-CATATG-3′ through a combination of sequence-dependent twistability and direct readout by the guanidinium moieties in the DNA major groove. This target site for Λ-1-$[Rh(MGP)_2phi]^{5+}$ is not a strong site for reaction by Λ-$[Rh(phen)_2phi]^{3+}$. Instead, the presence of the ancillary

(24) This observation suggests that Δ-1-$[Rh(GEB)_2phi]^{5+}$, like Δ-1-$[Rh(MGP)_2phi]^{5+}$, may be canted in its binding site.[4]

(25) Pyle, A. M.; Rehmann, J. P.; Meshoyrer, R.; Kumar, C. V.; Turro, N. J.; Barton, J. K. *J. Am. Chem. Soc.* **1989**, *111*, 3051.

Scheme 3. One-Pot Synthesis of $[Rh(MGP)_2Phi]Cl_5$ (**19**)[a]

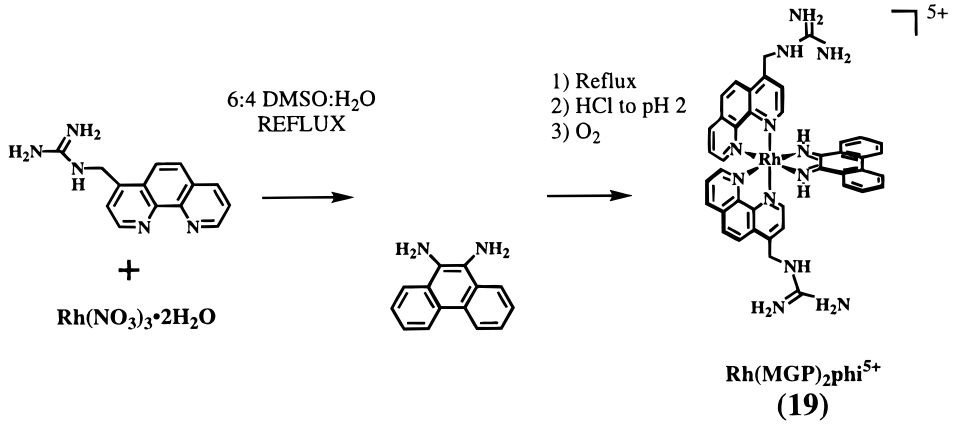

[a] A similar procedure was used for the syntheses of $[Rh(amidoEB)_2Phi]Cl_3$ (**20**), $[Rh(aminoPB)_2Phi]Cl_5$ (**21**), $[Rh(GEB)_2Phi]Cl_5$ (**22**), and $[Rh(GPB)_2Phi]Cl_5$ (**23**) except $RhCl_3 \cdot xH_2O$ was used instead of $Rh(NO_3)_3 \cdot xH_2O$.

guanidinium groups on the complex allows for specific hydrogen bonding with guanine residues at the first and sixth base pair positions, and strong stabilization *only* if the target site is sufficiently unwound (70 degrees) to present the guanine bases in a geometry which accommodates these interactions.[26] This necessity for unwinding to achieve hydrogen bonding is supported by the stringent requirement for the central 5′-TA-3′ step. Recognition of adenine in the first and sixth position (targeting 5′-TATATA-3′), while somewhat lowered in intensity compared to the primary site, is still possible since hydrogen bonding of the ancillary guanidinium moieties to the adenine N7 atoms positioned in a similarly unwound conformation still offers stabilization.

For the Δ-isomer, we propose that, as for Λ-isomer, site-specificity is based upon direct readout of guanine residues by the ancillary guanidinium functionalities on the complex. The two isomers bind their target sites with comparable affinities. Additionally the primary site targeted by Δ-1-$[Rh(MGP)_2phi]^{5+}$ represents a strong site for the parent $[Rh(phen)_2phi]^{3+}$, shown earlier to bind by intercalation from the major groove.[6,27] However, in this respect recognition by Δ-1-$[Rh(MGP)_2phi]^{5+}$ differs from that of the Λ-isomer. The observed cleavage for the family of phi complexes indicates for 1-Δ-$[Rh(MGP)_2phi]^{5+}$ the presence of the guanidinium groups arranged toward the DNA offers an added source of stabilization. This effect is demonstrated in photocleavage comparisons of 1-Δ-$[Rh(MGP)_2phi]^{5+}$, 2-Δ-$[Rh(MGP)_2phi]^{5+}$, and $[Rh(phen)_2phi]^{3+}$; while 2-Δ-$[Rh(MGP)_2phi]^{5+}$ shows a higher intensity of photocleavage compared to $[Rh(phen)_2phi]^{3+}$ across the fragment, there is no preferential enhancement at the target site for 1-Δ-$[Rh(MGP)_2phi]^{5+}$, 5′-CATCTG-3′.[14] Hence, unlike for the Λ-isomer, adding functionality onto the Δ-enantiomer stabilizes a subset of $[Rh(phen)_2phi]^{3+}$ target site(s). Interestingly, the hierarchy for recognition of outer sequences by the Δ-isomer parallels that by the Λ-isomer (Table 1). For Δ-1-$[Rh(MGP)_2phi]^{5+}$, based upon molecular model building, one would expect that a substantial amount of unwinding is not needed to orient the guanidinium functionalities of the right-handed metal complex for hydrogen bonding in the major groove of the right-handed DNA helix. A central 5′-TA-3′ is therefore not required. As for the Λ-isomer, however, one would expect the outer sequence heirarchy to be maintained, that is the preferred sites to contain guanines in the first and sixth positions, with adenines as secondary, somewhat weaker alternatives. Model building also suggests that the preference for two pyrimidines in the center of the target site may arise from steric interactions with the phenanthrolines.

Λ-1-$[Rh(MGP)_2phi]^{5+}$ and Δ-1-$[Rh(MGP)_2phi]^{5+}$, therefore, each target 6-base pair sequences with high affinity and specificity. This specificity is derived chiefly from interactions of the pendant guanidinium groups with the DNA bases. However, how those interactions are accomplished structurally differs between the two isomers.

Alternate Functionalities. Analogous site-specificity or isomer-specificity is not evident with the complexes which contain pendant amido or amino functionalities. Instead, these complexes appear to resemble the parent, unfunctionalized $[Rh(phen)_2phi]^{3+}$ with respect to recognition. For $[Rh(aminoPB)_2phi]^{5+}$, a small increase in cleavage intensity was apparent compared to $[Rh(phen)_2phi]^{3+}$, but the pattern of cleavage was the same. We attribute this increase to a nonspecific effect, likely associated with the increase in charge on the pendant amino group. Indeed, here the enhancement is evident more for the 2-positional isomer in which the functionality is disposed away from rather than toward the DNA groove.

The absence of new specificity for the amido functionalized complex was somewhat surprising and may reflect the lower degree of stabilization associated with amide−base interactions compared with guanidinium−base interactions. It is nonetheless difficult to draw any conclusions given the absence of an effect, and such a lack of effect may also reasonably be associated with poor positioning of the functionality with respect to the DNA bases and/or the flexibility of the linker.

Positioning of Guanidinium Functionalities with Different Linkers. The inherent utility of the guanidinium moiety in establishing specific base interactions is evident in the similar photocleavage patterns for the racemates of 1-$[Rh(MGP)_2phi]^{5+}$, 1-$[Rh(GEB)_2phi]^{5+}$, and 1-$[Rh(GPB)_2phi]^{5+}$, a series in which all complexes contain the guanidinium functionality, but through a linker differing in length and flexibility. The patterns are nearly identical for this family with the strongest site of photocleavage being 5′-CATCTG-3′. Moreover, for each of these complexes, enhanced photocleavage is evident for the 1-positional isomer compared to the 2-positional isomer. This observation supports

(26) Whether the complex traps the target site in an unwound conformation or helps to induce the unwound structure has not been established.
(27) NMR studies of Δ-1-$[Rh(MGP)_2phi]^{5+}$ bound to 5′-CGCATCTGAC-3′ supports intercalation in the major groove. Franklin, S.; Barton, J. K. *Biochemistry* in press.
(28) Newkome, G.; Lee, H.-W. *J. Am. Chem. Soc.* **1983**, *105*, 5956.

the idea that the enhancement results not from increased electrostatics but specific hydrogen bonding.

More subtle differences that can be attributed to the linker are evident in photocleavage studies with enantiomers of the axial geometric isomer (1). For Δ-1-$[Rh(MGP)_2phi]^{5+}$ strongest cleavage is evident at 5′-CATCTG-3′ while Δ-1-$[Rh(GEB)_2phi]^{5+}$ shows approximately equal intensity at that site and 5′-GATCTC-3′; this observation may be associated with the greater flexibility in the linker arm for Δ-1-$[Rh(GEB)_2phi]^{5+}$. More interesting are the differences evident in recognition by the Λ-isomers. While Λ-1-$[Rh(MGP)_2phi]^{5+}$ displays significant photocleavage at 5′-CATATG-3′, Λ-1-$[Rh(GEB)_2phi]^{5+}$ shows little cleavage at this site. Hence, lengthening of the linker by one carbon greatly decreases affinity (or photoefficiency) at this site. This sensitivity to linker length may be associated with the mode of recognition of 5′-CATATG-3′, involving sequence-dependent unwinding of the DNA site. Thus strategies for recognition which involve sequence-dependent variations in DNA conformation coupled to direct read-out may be particularly sensitive to proper alignment of functionality.

Implications for Design. The construction of the series of complexes with functional additions to $[Rh(phen)_2phi]^{3+}$ and $[Rh(bpy)_2phi]^{3+}$ and the examination of DNA recognition by the different isomers generated has yielded some new and valuable insights with respect to predictable design strategies. First and foremost, DNA site recognition is most sensitive to stereochemical placement of functionality along the DNA helix. Metallointercalation offers a means to orient functionality with respect to the DNA helical axis. Metallointercalation furthermore offers a means to achieve DNA binding with high affinity. In addition, guanidinium functionalities have been seen to be most effective in establishing site-specific contacts. Indeed when guanidinium moieties are appended without great flexibility onto the $[Rh(phen)_2phi]^{3+}$ core, sequence-specific recognition on the 6-base pair level is observed. Importantly, this recognition depends sensitively upon stereochemical placement. Pendant guanidinium functionalities therefore appear to be particularly advantageous in the construction of small molecules which bind DNA with site-specificity.

Acknowledgment. We are grateful to the NIH (GM33309) for their financial support of this research and for NRSA training support (R.H.T. and T.W.J.). We also thank Daniel Hall and Dr. Masako Kato for their contributions to optimizing the syntheses and Duncan Odom for manuscript preparation.

Supporting Information Available: Experimental details of the synthesis of all ligands and metal complexes (7 pages). Ordering information is given on any current masthead page.

IC980837J